(Received 4 February 2024, Accepted 8 July 2024, Scheduled 14 July 2024)

High-Performance Ceramic Filter Design Based on Six-Blind-Hole Coupling Structure

Yang Gao[1], Yunxiu Wang[1,*], Xiaotao Yao[1], Guangyong Wei[1], and Jie Liu[2]

[1] *School of Electronic and Information Engineering, China West Normal University, Nanchong 637009, China*
[2] *School of Physics and Astronomy, China West Normal University, Nanchong 637009, China*

ABSTRACT: An innovative ceramic filter is presented in this paper. The filter is composed of six tuning apertures, coupling channels, and a six-blind-hole coupling structure. The six blind holes are divided into two groups: one situated between the first and second cavities to induce inductive coupling, and the other positioned between the second and third cavities to facilitate capacitive coupling. Employing this structure facilitates the formation of a cascade quadruple (CQ) coupling unit among the 1, 2, 3, and 4 resonant cavities, thereby introducing two transmission zeros. Subsequently, an analysis of the influences of the depth and spacing of each blind hole on the coupling coefficients is presented. Finally, to further validate the theory, the filter tailored for base station applications was designed and implemented. The measurement results demonstrate a center frequency of 3.5 GHz with a bandwidth of 200 MHz. In the passband, the insertion loss was below 1.2 dB, and the return loss surpassed 19 dB. The test outcomes align closely with the simulation, confirming the reliability of the design.

1. INTRODUCTION

With the development of 5G communication technology, a large number of microwave base stations need to be built. Ceramic filters have been widely concerned in recent years due to their light weight, compact size, high Q-factor, and stable performance. Miniaturization and high performance are two issues that need special attention in filter design [1–10]. In the design of ceramic medium filters, capacitive coupling is widely employed because it can form a cascade quadruple (CQ) structure in conjunction with inductive coupling, introducing transmission zeros to enhance the filter's selectivity while reducing its size and weight [11–19]. The authors in [16] first proposed a capacitive coupling structure composed of a single-blind hole. Due to its structural simplicity, the design has been widely adopted in the field. The required performance can be achieved by merely adjusting the depth of the hole, although high precision in manufacturing is necessary. In another literature [18], stepped through-holes are employed which consist of two cylindrical holes with different radii. The depth of the larger cylindrical hole is greater than half the height of the filter. The inner wall of the larger cylindrical hole is coated with metal, while the smaller cylindrical hole is not coated. The coupling coefficients can be conveniently adjusted by varying the depth of cylindrical holes. As reported in [19], the authors designed a ten-order ceramic waveguide filter that used a microstrip electrical coupling structure. The design features a square notch between resonators with added metal lines. While some electromagnetic leakage is present, this approach offers a novel perspective on filter design. In [13], the authors proposed a negative coupling structure with conical through-hole consisting of a cylindrical hole and a conical hole. The coupling bandwidth can be adjusted flexibly by altering the coated area of the conical hole and the depth of the cylindrical hole, addressing the defect of limited electric coupling bandwidth range. However, this design exhibits relatively higher insertion loss.

In this paper, a six-cavity ceramic waveguide filter is designed based on two pairs of three-blind-hole coupling structures. One group is capacitive coupling while the other sgroup realizes inductive coupling. The capacitive or inductive coupling can be achieved by adjusting the relative depths of the central blind hole (h_s) and the two side blind holes (h_m), thus generating two transmission zeros to ensure that the filter has a high selectivity.

2. DESIGN AND ANALYSIS

Firstly, a six-blind-hole coupling structure is introduced, shown in Figure 1(a) which has wide out-of-band rejection characteristics. The filter incorporates six tuning holes, wherein resonators 1 and 2 are coupled by an inductive three-blind-hole. Simultaneously, a capacitive three-blind-hole structure realizes the coupling of resonators 2 and 3. The coupling through-slots are strategically employed among the remaining resonators to meet the required coupling coefficients. The overall size of the filter is 30.6 mm × 16.8 mm × 6 mm.

The CQ structure composed of resonators 1, 2, 3, and 4 with tuning holes in the middle can introduce two transmission zeros which significantly enhances the out-of-band rejection and debugging accuracy. Six tuning holes increase the convenience of later tuning.

The adopted topology is visually represented in Figure 1(b), where resonators 2 and 3 are capacitively coupled denoted by a

* Corresponding author: Yunxiu Wang (627662147@qq.com).

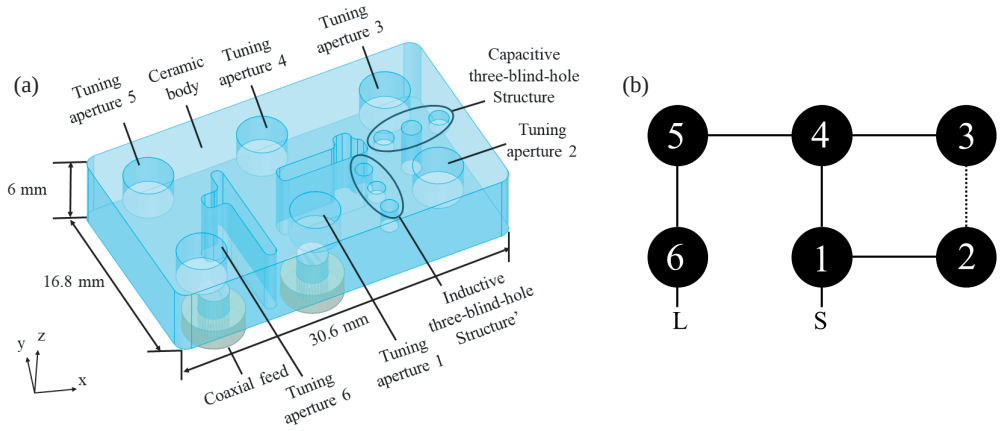

FIGURE 1. The six-cavity filter. (a) Structure diagram. (b) Topology structure.

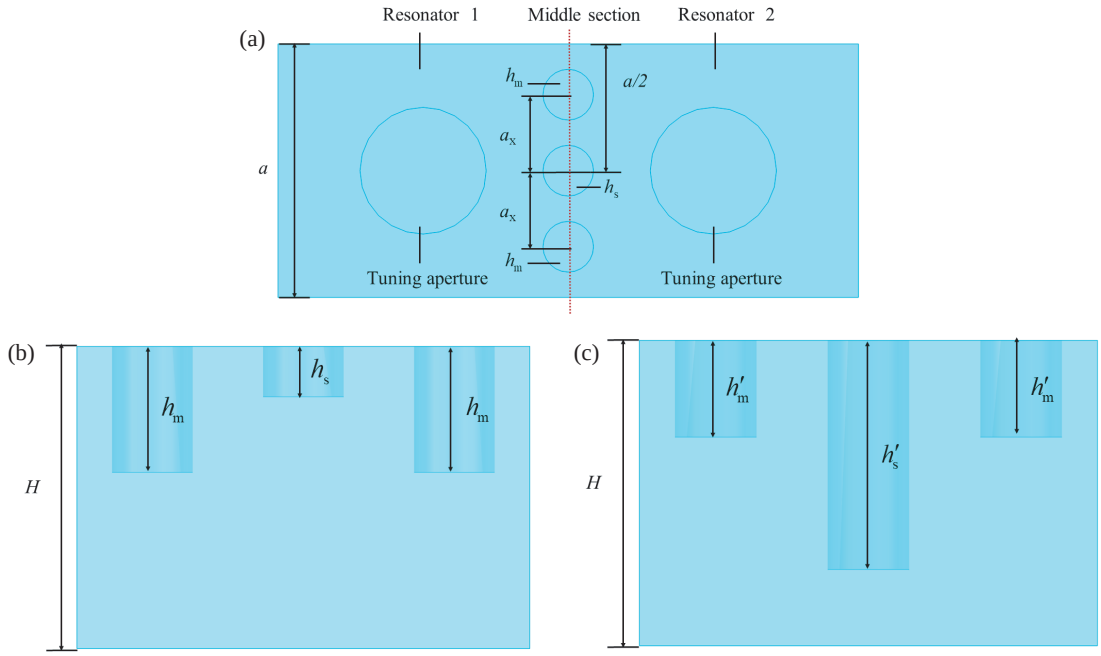

FIGURE 2. (a) Top view of three-blind-hole. (b) Inductive coupling. (c) Capacitive coupling.

dotted line, while the other tuning holes exhibit inductive coupling represented by a solid line. Resonator 1 is linked to the input port, and resonator 6 is connected to the output port.

2.1. Design of Six-Blind-Hole and The Coupling Through-Slots

As illustrated in Figure 2(a), the depth of the central blind hole is denoted as h_s, while the other two blind holes are labeled as h_m, and the distance between three blind holes is defined as a_x.

To ascertain the type of the three-blind-hole coupling, the two-mode extraction method [9] can be employed, as depicted in Equation (1), and f_e represents the resonant frequency of the main mode when the middle section is the ideal electric wall, while f_m is the resonant frequency of main mode as the middle section is the ideal magnetic wall. The k values can be extracted using electromagnetic simulation software [20] with the formula mentioned.

$$k = \frac{f_{\mathrm{e}}^2 - f_{\mathrm{m}}^2}{f_{\mathrm{e}}^2 + f_{\mathrm{m}}^2} \tag{1}$$

where $k > 0$ represents the inductive coupling, and $k < 0$ denotes the capacitive coupling.

Table 1 categorizes the parameter changes of inductive and capacitive coupling. Figure 3(a) shows the simulation results when $h_s = 2.0, 2.5, 3.0\,\mathrm{mm}$, $a_x = 1.6 \sim 2.8\,\mathrm{mm}$, and $h_m = 3\,\mathrm{mm}$ remains constant, which corresponds to Scheme 1 in Table 2. Similarly, Figures 3(b) $\sim$ (d) match Scheme 2 $\sim$ 4 in Table 2. Simulation results indicate that the three-blind-hole structure manifests inductive coupling when $h_{\mathrm{s}} < h_{\mathrm{m}} < H/2$, shown as in Figure 2(a). We can note from Figure 2(b) that it will present capacitive coupling as $h'_{\mathrm{s}} > h'_{\mathrm{m}}$ ($h'_{\mathrm{s}} > H/2$, $h'_{\mathrm{m}} < H/2$), here $4\,\mathrm{mm} < h'_s < 5.2\,\mathrm{mm}$.

TABLE 1. Design proposal.

	Inductive coupling							Capacitive coupling						
	Scheme 1			Scheme 2				Scheme 3			Scheme 4			
a_x (mm)	1.6 ∼ 2.8			1.6 ∼ 2.8			a'_x (mm)	1.6	2.1	2.6	2.2			
h_s (mm)	2.0	2.5	3.0	1.0			h'_s (mm)	4.0 ∼ 5.2			4.0 ∼ 5.2			
h_m (mm)	3.0			2.0	2.5	3.0	h'_m (mm)	3.0			1.0	2.0	3.0	

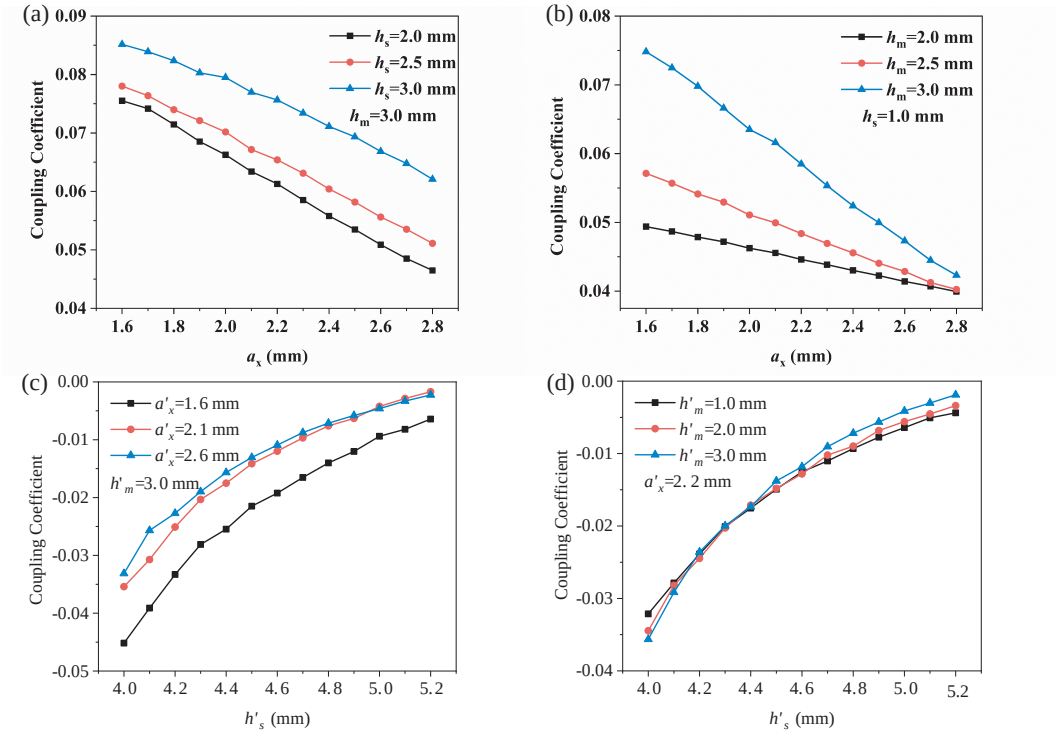

FIGURE 3. Simulated coupling coefficient of the three-blind-hole. (a) Scheme 1. (b) Scheme 2. (c) Scheme 3. (d) Scheme 4.

L and W are used to denote the length and width of the coupling through-slot in Figure 4(a). Figures 4(b) and 4(c) indicate that the decrease in the coupling coefficient is caused by the increase of L and W.

2.2. Design of Feed Structure and Tuning Holes

The classic coaxial feed method is employed for both input and output ports. The extent of coupling between the source or load and the neighboring cavities is quantified by the Q_e value. Q_e is calculated by using the group delay method [13] with the following equation:

$$Q_{\mathrm{e}} = \frac{\omega_0 \tau_{\max}}{4} \tag{2}$$

where $\tau_{\max}$ is the maximum group delay at resonance, and ω_0 represents the angular frequency corresponding to the maximum group delay.

In Figure 5(a), H_T and H_p are used to denote the depth of the tuning aperture and the feeding depth of the probe. The initial depth of the tuning aperture H_T is set to 2.77 mm when the main mode resonance frequency is at 3.5 GHz. By changing H_T, the relationship between the center frequency f_0 and H_T is obtained as shown in Figure 5(b). It can be seen that as H_T increases, the resonant frequency will decrease.

It can be observed from Figure 5(c) that Q_e decreases when H_p increases.

2.3. Design of Six-Cavity Ceramic Waveguide Filter

First, the Filter Designer 3D software [21] can be used to select the appropriate topology and normalized coupling matrix M based on the specifications in Table 2. The formula for calculating the relative bandwidth is as follows:

$$FBW = \frac{f_2 - f_1}{f_0} \tag{3}$$

where $f_2 = 3.6\,\mathrm{GHz}$ and $f_1 = 3.4\,\mathrm{GHz}$ respectively correspond to the upper and lower frequency points of the passband where the attenuation is 3 dB. Thereby FBW is calculated as 0.0571. The actual coupling matrix K is equal to M multiplying FBW. That is

$$K = M \times FBW$$

TABLE 2. The technical specifications.

Design Parameters	Indicators
f_0 (GHz)	3.5
FBW (%)	5.7
IL (dB)	≤ 1.2
RL (dB)	≥ 16
Group Delay (ns)	≤ 20 within 3.4 GHz $\sim$ 3.6 GHz
near-end out-of-band suppression (dB)	≥ 25 within 3.3 $\sim$ 3.35 GHz and 3.65 $\sim$ 3.7 GHz
far-end out-of-band suppression (dB)	≥ 51 within 3.2 $\sim$ 3.3 GHz and 3.7 $\sim$ 3.8 GHz

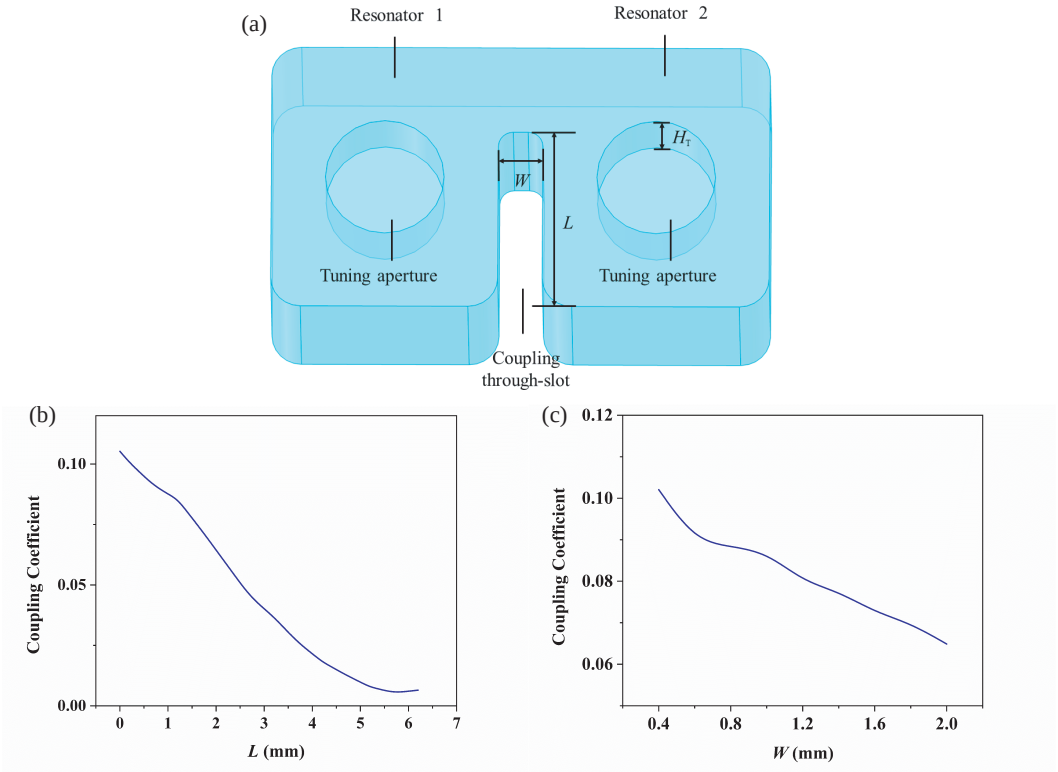

FIGURE 4. (a) The diagram of the coupling through-slot. (b) The relationship between coupling coefficient and L. (c) The relationship between coupling coefficient and W.

$$= \begin{bmatrix} 0 & 0.0605 & 0 & 0 & 0 & 0 & 0 & 0 \\ 0.0605 & 0 & 0.0507 & 0 & 0.0055 & 0 & 0 & 0 \\ 0 & 0.0507 & 0 & -0.0393 & 0 & 0 & 0 & 0 \\ 0 & 0 & -0.0393 & 0 & 0.0331 & 0 & 0 & 0 \\ 0 & 0.0055 & 0 & 0.0331 & 0 & 0.0357 & 0 & 0 \\ 0 & 0 & 0 & 0 & 0.0357 & 0 & 0.0510 & 0 \\ 0 & 0 & 0 & 0 & 0 & 0.0510 & 0 & 0.0605 \\ 0 & 0 & 0 & 0 & 0 & 0 & 0.0605 & 0 \end{bmatrix} \quad (4)$$

The single-cavity model is initially established in the HFSS simulation software. Based on the previously determined topology structure and the actual coupling matrix K, appropriate coupling structures are selected to establish the overall model. In this work, six-blind-holes and a coupling through-slot are adopted as the coupling structure of the filter, while the input and output ports utilize coaxial feeding. Subsequently, the initial dimensions of the coupling structure and feeding structure are determined based on the calculated actual coupling matrix K.

The filter debugging applies the parameter extraction method. Initially, S-parameters are extracted from HFSS and imported into Filter Design 3D to generate the error matrix. Subsequently, the filter geometry is adjusted based on the error matrix until the ideal coupling matrix K is achieved. Figure 6 illustrates the optimized physical dimensions. The specific parameters are outlined in Table 3.

3. FILTER FABRICATION AND MEASUREMENT

Figure 7 shows photos of the fabricated filter. The ceramics have a relative permittivity of 20.3 and a loss tangent of 1.4×10^{-4}. The accuracy is 0.02 mm on the outer surface, and the depth of the hole is 0.03 mm.

The filter was characterized using the ZNB40 network analyzer, as depicted in Fig. 8(a). The center frequency is 3.5 GHz, bandwidth 200 MHz, and return loss $\geq$ 19 dB. The inser-

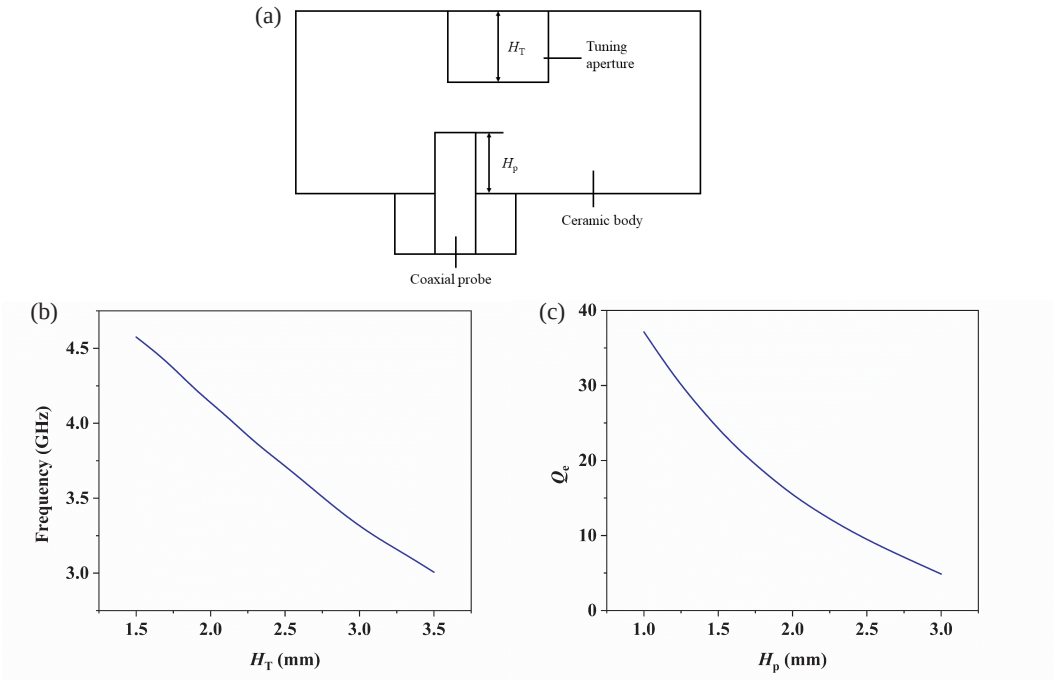

FIGURE 5. (a) The diagram between the source or load and the resonator. (b) The relationship between resonance frequency and H_T. (c) The relationship of Q_e and H_p.

Symbol	Value	Symbol	Value	Symbol	Value
H_{T1}	2.66	$L1$	7.65	h_m	2.30
H_{T2}	2.71	$L2$	1.10	a_x	2.20
H_{T3}	2.75	$L3$	2.96	h'_s	4.42
H_{T4}	2.56	$L4$	9.49	h'_m	0.80
H_{T5}	2.52	H_{P1}	2.00	a'_x	2.40
H_{T6}	2.64	H_{P2}	2.00		
W	1.50	h_s	1.00		

TABLE 3. Parameters of the filter (in mm).

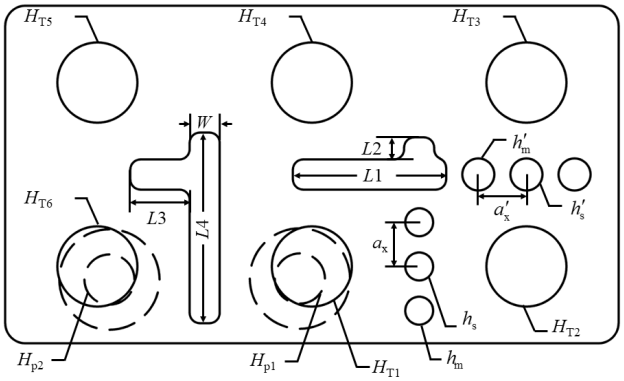

FIGURE 6. The optimized structure of the six-cavity waveguide filter.

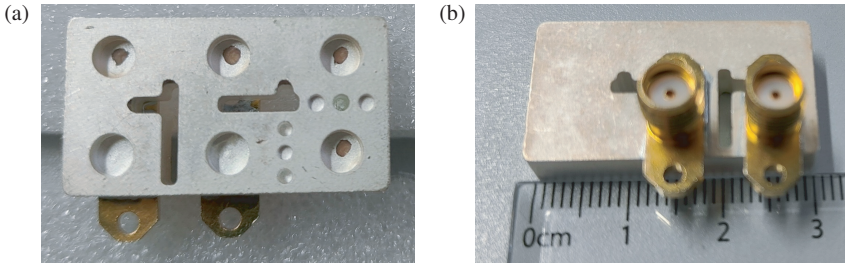

FIGURE 7. The manufactured six-cavity ceramic waveguide filter. (a) Top surface view. (b) Bottom surface view.

tion loss remains $\leq$ 1.2 dB within 3.4 $\sim$ 3.6 GHz. Furthermore, within 3.2 $\sim$ 3.3 GHz and 3.7 $\sim$ 3.8 GHz, the filter demonstrates remarkable suppression ($\geq$ 55 dB). Within 3.3 $\sim$ 3.35 GHz and 3.65 $\sim$ 3.7 GHz, the suppression effects are $\geq$ 28 dB. It is shown in Figure 8(b) that the in-band group delay is $\leq$ 20 ns.

Upon comparing the simulation and test results, it is evident that they are relatively consistent, affirming the feasibility and accuracy of the design. However, there is a discrepancy between the measured values of return loss and insertion loss and the simulated results, primarily due to computational errors in the simulation software, limitations in manufacturing precision,

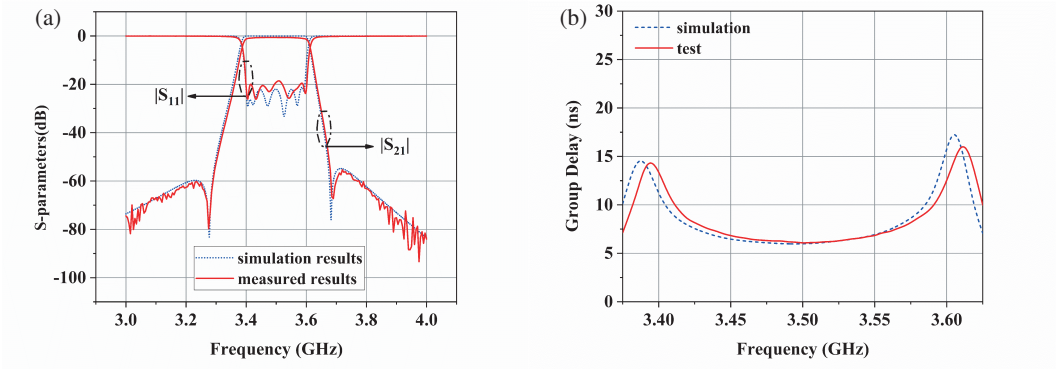

FIGURE 8. The experimental and simulation results. (a) S-parameters. (b) Group delay.

TABLE 4. The comparison between designed filter and other 5G base station filters.

Ref.	[19]	[13]	[14]	[22]	[23]	[11]	This work
Order	10	8	6	6	6	6	6
f_0 (GHz)	2.595	3.5	3.5	3.458	3.5	3.5	3.5
FBW (%)	6.2	5.7	5.7	5.7	6.56	5.7	5.7
IL (dB)	≤ 2.2	≤ 2	≤ 2	≤ 1.2	≤ 2	≤ 1.2	≤ 1.2
RL (dB)	≥ 20	≥ 19	≥ 17	≥ 17.5	≥ 16	≥ 17	≥ 19
Group Delay (ns)	≤ 30	≤ 25	≤ 20	≤ 20	≤ 20	≤ 20	≤ 20
near-end out-of-band suppression (dB)	≥ 40	≥ 39	≥ 15	≥ 20	≥ 25	≥ 25	≥ 28
far-end out-of-band suppression (dB)	≥ 65	≥ 63	≥ 20	≥ 17	≥ 45	≥ 51	≥ 55
Volume (cm^3)	6.996	4.788	15.6	11.063	4.967	3.162	3.084

and uncertainties in the silver layer etching process. Additionally, the proximity of the three blind holes during the manufacturing process may lead to additional fabrication challenges. To address this issue, future research could consider adjusting the layout of the three blind holes, for example, by placing the two side holes on the upper surface and the central hole on the lower surface, or vice versa. This change in layout not only alleviates the fabrication difficulties associated with the narrow spacing between the blind holes but also provides greater flexibility in filter design.

Table 4 is the comparison between other ceramics filters and the proposed one. The six-cavity ceramic waveguide filter designed exhibits superior near-end and far-end out-of-band suppression performance compared to other six-cavity filters. Concurrently, its size is relatively smaller than other filters.

4. CONCLUSION

Based on the six-blind-hole coupling structure, a novel six-cavity ceramic waveguide filter is designed. A detailed analysis is conducted on the impact of the depth and distance of each blind hole in the two groups of blind holes on the coupling coefficients. Through simulations and measurements, the feasibility and correctness of the design are further validated. The filter has high performance and compact size which is suitable for 5G base stations and other prospects of practical applications.

ACKNOWLEDGEMENT

This work was supported by the Fundamental Research Funds of China West Normal University.

REFERENCES

[1] Wang, X., G. Jang, B. Lee, and N. Park, "Compact quad-mode bandpass filter using modified coaxial cavity resonator with improved Q-factor," *IEEE Transactions on Microwave Theory and Techniques*, Vol. 63, No. 3, 965–975, Mar. 2015.

[2] Chen, F., X. Li, Y. Zhang, and Y. Jiang, "Design and implementation of initial cell search in 5G NR systems," *China Communications*, Vol. 17, No. 5, 38–49, May 2020.

[3] Liu, S. and G. Gan, "Novel DDS based OFDM transmitter structure without IFFT and interpolation filter," *China Communications*, Vol. 18, No. 12, 219–229, 2021.

[4] Carceller, C., F. Gentili, W. Bösch, D. Reichartzeder, and M. Schwentenwein, "Ceramic additive manufacturing as an alternative for the development of miniaturized microwave filters," in *2017 IEEE MTT-S International Microwave Workshop Series on Advanced Materials and Processes for RF and THz Applications (IMWS-AMP)*, 1–3, Pavia, Italy, 2017.

[5] Hendry, D. R. and A. M. Abbosh, "Triple-mode ceramic cavity filters with wide spurious-free performance," *IEEE Transactions on Microwave Theory and Techniques*, Vol. 65, No. 10, 3780–3788, 2017.

[6] Hendry, D. R. and A. M. Abbosh, "Compact high-isolation base-station duplexer using triple-mode ceramic cavities," *IEEE*

Transactions on Industrial Electronics, Vol. 65, No. 10, 8092–8100, 2018.

[7] Hendry, D. R. and A. M. Abbosh, "Compact triple-mode band-stop ceramic cavity filters using parallel coupled resonators," *IEEE Microwave and Wireless Components Letters*, Vol. 29, No. 8, 526–528, 2019.

[8] Fiedziuszko, S. J., I. C. Hunter, T. Itoh, Y. Kobayashi, T. Nishikawa, S. N. Stitzer, and K. Wakino, "Dielectric materials, devices, and circuits," *IEEE Transactions on Microwave Theory and Techniques*, Vol. 50, No. 3, 706–720, Mar. 2002.

[9] He, Y., "Research on high performance ceramic dielectric filter," University of Electronic Science and Technology of China, Sichuan, China, 2022.

[10] Levy, R., "Direct synthesis of cascaded quadruplet (CQ) filters," *IEEE Transactions on Microwave Theory and Techniques*, Vol. 43, No. 12, 2940–2945, 1995.

[11] Liang, F., S. Meng, and W. Lyu, "Design of microwave ceramic waveguide filter with high out-of-band suppression characteristics," *Journal on Communications*, Vol. 42, No. 04, 194–201, 2021.

[12] Meng, S., F. Liang, Z. Lin, W. Lu, and X. Wang, "Design of six-cavity ceramic waveguide filter with four transmission zeros," in *2021 IEEE 4th International Conference on Electronic Information and Communication Technology (ICEICT)*, 304–307, Xi'an, China, 2021.

[13] Meng, S., F. Liang, W. Lu, Z. Lin, Y. Yin, and R. Zhang, "Design of a microwave filter based on a novel negative coupling structure with conical through-hole," *China Communications*, Vol. 19, No. 2, 148–157, Feb. 2022.

[14] Chen, Y. and K.-L. Wu, "An all-metal capacitive coupling structure for coaxial cavity filters," in *2020 IEEE/MTT-S International Microwave Symposium (IMS)*, 583–586, Los Angeles, CA, USA, 2020.

[15] Latif, M., G. Macchiarella, and F. Mukhtar, "A novel coupling structure for inline realization of cross-coupled rectangular waveguide filters," *IEEE Access*, Vol. 8, 107 527–107 538, 2020.

[16] Bengui, Y., "Dielectric filter, transceiver, and base station," US Patent App. 16/899, 027, 2020.

[17] Hu, H. and K.-L. Wu, "A TM11 dual-mode dielectric resonator filter with planar coupling configuration," *IEEE Transactions on Microwave Theory and Techniques*, Vol. 61, No. 1, 131–138, 2012.

[18] Wei, B. and R. F. Shun, "Dielectric filter," CN209434356U, Dec. 2019.

[19] Du, Z., J. Pan, X. Ji, D. Yang, and X. Liu, "Ceramic dielectric-filled cavity filter," in *2020 IEEE 5th Information Technology and Mechatronics Engineering Conference (ITOEC)*, 888–891, Chongqing, China, 2020.

[20] Ansys, Available: www.ansys.com.

[21] CST Studio Suite, Available: www.cst.com.

[22] Mao, D. X., "Design of dielectric waveguide filter for 5G applications," Nanjing University of Posts and Telecommunications of China, Nanjing, China, 2021.

[23] Zhang, S., "Design and research of cross-coupled dielectric waveguide filter for 5G applications," Nanjing University of Posts and Telecommunications of China, Nanjing, China, 2023.